Contrib Mineral Petrol (2005) 149: 129–140
DOI 10.1007/s00410-004-0646-3

ORIGINAL PAPER

Bernardo Cesare · Sandro Meli · Luca Nodari
Umberto Russo

Fe^{3+} reduction during biotite melting in graphitic metapelites: another origin of CO_2 in granulites

Received: 15 April 2004 / Accepted: 2 December 2004 / Published online: 3 February 2005

Abstract The Fe^{3+}/Fe_{tot} of all Fe-bearing minerals has been analysed by Mössbauer spectroscopy in a suite of biotite-rich to biotite-free graphitic metapelite xenoliths, proxies of an amphibolite-granulite transition through progressive biotite melting. Biotite contains 9 to 16% Fe^{3+}/Fe_{tot}, whereas garnet, cordierite and ilmenite are virtually Fe^{3+} -free (0–1% Fe^{3+}/Fe_{tot}) in all samples, regardless of biotite presence. Under relatively reducing conditions (graphite-bearing assemblages), biotite is the only carrier of Fe^{3+} during high-temperature metamorphism; therefore, its disappearance by melting represents an important event of iron reduction during granulite formation, because haplogranitic melts usually incorporate small amounts of ferric iron. Iron reduction is accompanied by the oxidation of carbon and the production of CO_2, according to the redox reaction:

$$2Fe_2O_3^{(Bt)} + C^{(Gr)} \Rightarrow 4FeO^{(Crd,Grt,Ilm,Opx)} + CO_2^{(fluid,melt,Crd)}.$$

Depending on the nature of the peritectic Fe-Mg mineral produced (garnet, cordierite, orthopyroxene), the CO_2 can either be present as a free fluid component, or be completely stored within melt and cordierite. The oxidation of graphite by iron reduction can account for the in situ generation of CO_2, implying a consequential rather than causal role of CO_2 in some granulites and migmatites. This genetic model is relevant to graphitic rocks more generally and may explain why CO_2 is present in some granulites although it is not required for their formation.

Editorial Responsibility: J.L.R. Touret

B. Cesare
Dipartimento di Mineralogia e Petrologia,
Università di Padova, Corso Garibaldi, 37,
35137 Padova, Italy

B. Cesare (✉)
CNR, Istituto di Geoscienze e Georisorse,
Sezione di Padova, Corso Garibaldi, 37,
35137 Padova, Italy
E-mail: bernardo.cesare@unipd.it
Tel.: +39-49-8272019
Fax: +39-49-8272010

S. Meli
Dipartimento di Scienze della Terra,
Università di Parma, Parco Area delle Scienze 157a,
43100 Parma, Italy

L. Nodari · U. Russo
Dipartimento di Scienze Chimiche,
Università di Padova, Via Marzolo, 1,
35131 Padova, Italy

Introduction

Granulites play a key role in the processes of high-grade metamorphism, granite genesis and crustal differentiation (Harley 1989; Clemens 1990; Vielzeuf et al. 1990). Owing to their general anhydrous character and to the presence - in addition to saline brines - of CO_2-rich fluid inclusions (e.g. Touret 1971; 1981), a relationship between CO_2-rich fluids and granulite genesis has often been proposed, leading to the concept of "carbonic metamorphism" (Newton et al. 1980; Peterson and Newton 1989; Santosh 1992). However, it is now accepted by most researchers that CO_2 infiltration cannot cause melting and formation of large volumes of granulites (e.g., Clemens 1993), and only produces melt-absent dehydration along channelled pathways (Valley et al. 1983; Farquhar and Chacko 1991). If it is also considered that the mobility of CO_2 along grain boundaries is very low (Watson and Brenan 1987), one is faced with one of the most intriguing controversies in metamorphic petrology: why is CO_2 ubiquitous in granulites if it is not required for their formation and not able to percolate through rocks? This question is still unanswered, and the role and origin of CO_2 in granulites is still unclear (Brown 2003). Up to now, proposed sources of CO_2 are the degassing mantle, crystallising

mafic magmas, or metamorphosing carbonates (Valley et al. 1983; Frost and Frost 1987; Lamb et al. 1987; Clemens 1990). In most models CO_2 is believed to behave passively, concentrating in the fluid by selective partitioning of H_2O in the melt (e.g., Touret and Dietvorst 1984; Fitzsimons and Mattey 1994). There is also evidence that in some granulites CO_2 is late and postdates the peak of metamorphism (e.g., Lamb et al. 1987). Therefore, the most accepted views are that CO_2 is either causal or casual in the process of granulite formation: in fact even if CO_2 fractionation in the fluid can derive from anatexis and granulite formation, it requires that CO_2 was already present in the rock.

An alternative origin of CO_2—in situ generation by oxidation of graphite– was proposed by Touret (1971), based on the presence of graphite in metasedimentary granulites from Norway, and supported by C isotope data (Pineau et al. 1981). Later, Hollister (1988) proposed that graphite oxidation may be induced by biotite melting. Applying this model to the genesis of Opx-bearing migmatites (mineral abbreviations after Kretz 1983), he suggested that during high-temperature dehydration melting of biotite, CO_2 might form by reduction of Fe^{3+} and simultaneous oxidation of graphite. This model, which implies that CO_2 can be a consequence of granulite formation, has been generally overlooked in the subsequent literature. Here we explore the application of Hollister's idea to metasedimentary granulites and migmatites, which are frequently observed in many metamorphic terranes. This study started after the discovery that, similarly to lower-grade metapelites (Dyar et al. 2002 and references therein), biotite equilibrated at high temperature (850 ± 50°C) and under reducing conditions (ilmenite-graphite) may contain up to 16% Fe^{3+}/Fe_{tot} (Cesare et al. 2003a). Therefore we have analysed for Fe^{3+} all Fe-bearing minerals contained in rocks representative of an amphibolite-granulite transition in graphitic metapelites, with the aim of quantifying the Fe^{3+} balance during granulite formation.

The results of this research indicate that biotite melting represents an important event of iron reduction, which is able to produce significant amounts of CO_2 provided that also graphite is present in the rock. It follows that some occurrences of CO_2-rich fluids in granulites may be a natural consequence of granulite formation, which do not require the infiltration of external fluids.

Sample petrography

We chose the well-characterised crustal xenoliths from El Hoyazo, SE Spain, (Cesare et al. 2003a and references therein), which preserve extremely well the chemical features of partially melted rocks at mid-crustal conditions without having been subjected to retrograde re-equilibration, as commonly happens in many granulites (e.g., Brown 2002).

Three biotite-rich (HO20, HO30, HO50) and two biotite-poor to biotite-free xenoliths (HO03, AV-HZ8), all graphitic, were selected (Fig. 1). Their full mineral assemblages are listed in Table 1. The biotite-rich samples are the typical Bt-Grt-Sil xenoliths of El Hoyazo, where the crystal chemical features of biotite has been studied already (Cesare et al. 2003a). These medium-grained, foliated graphitic metapelites (Fig. 1a) partially melted at c. 850 ± 50°C, 7 kbar; biotite is still stable because of the absence of quartz and its high Ti content. These xenoliths do not contain fluid inclusions, but preserve abundant interstitial glass as well as fresh glass inclusions, which attest to an anatectic origin and the lack of post-peak retrograde phenomena. Xenoliths are also rich in disseminated graphite (Fig. 1b, see also Cesare and Maineri 1999). Of the three Bt-rich samples, only HO50 contains ilmenite, cordierite and K-feldspar (Table 1), all in minor amounts (< 1%), and displays some evidence of weathering of the interstitial glass. In the second group of xenoliths, HO03 and AV-HZ8, biotite is either absent or present as rare resorbed relics (Fig. 1c). Both samples contain cordierite and ilmenite, and disseminated graphite (Fig. 1d). The occurrence of primary melt inclusions in cordierite and ilmenite (Fig. 1d) indicates that these minerals have grown in the presence of (i.e., coexisting with) a melt phase. These microstructures, as well as the armouring of embayed biotite relics within cordierite (Fig. 1e) are suggestive of a melting reaction consuming biotite and forming cordierite and ilmenite. Sample AV-HZ8 shows similarities in grain-size, foliation style, graphite microstructures and mineral chemistry to the Bt-rich xenoliths. Therefore, although the occurrence as scattered fragments in the host lava cannot provide any field constraint, we infer that this sample may be genetically related to the Bt-rich ones via a reaction of biotite melting such as

$$\mathrm{Bt} + \mathrm{Pl} + \mathrm{Sil} \pm \mathrm{Grt} = \mathrm{melt} + \mathrm{Crd} + \mathrm{Ilm} \pm \mathrm{Kfs} \quad (1)$$

i.e., by a Qtz-absent, Ti-bearing modification of the model biotite dehydration melting reactions (Vielzeuf and Holloway 1988; Vielzeuf and Schmidt 2001):

$$\mathrm{Bt} + \mathrm{Sil} + \mathrm{Qtz} \pm \mathrm{Pl} = \mathrm{melt} + \mathrm{Crd} + \mathrm{Kfs} \quad (2)$$

An important feature of the Bt-poor samples is that cordierite and calcic plagioclase frequently contain carbonic fluid inclusions together with fresh melt inclusions of granitic composition (Fig. 1f), in microstructures which indicate the simultaneous entrapment of two "fluids" (carbonic and silicate melt) which were immiscible ("immiscible trapping", Roedder 1984). This is an extremely rare occurrence for crustal rocks and demonstrates that the fluid inclusions cannot have had a late, post-peak origin. Fluid inclusions have been characterised by microthermometry and laser Raman spectroscopy as CO_2-rich (> 80%), with minor amounts of CH_4, N_2, H_2 and CO (Cesare et al. 2004). As the inclusions display microstructures of primary entrapment, and as the nature of the xenoliths prevents

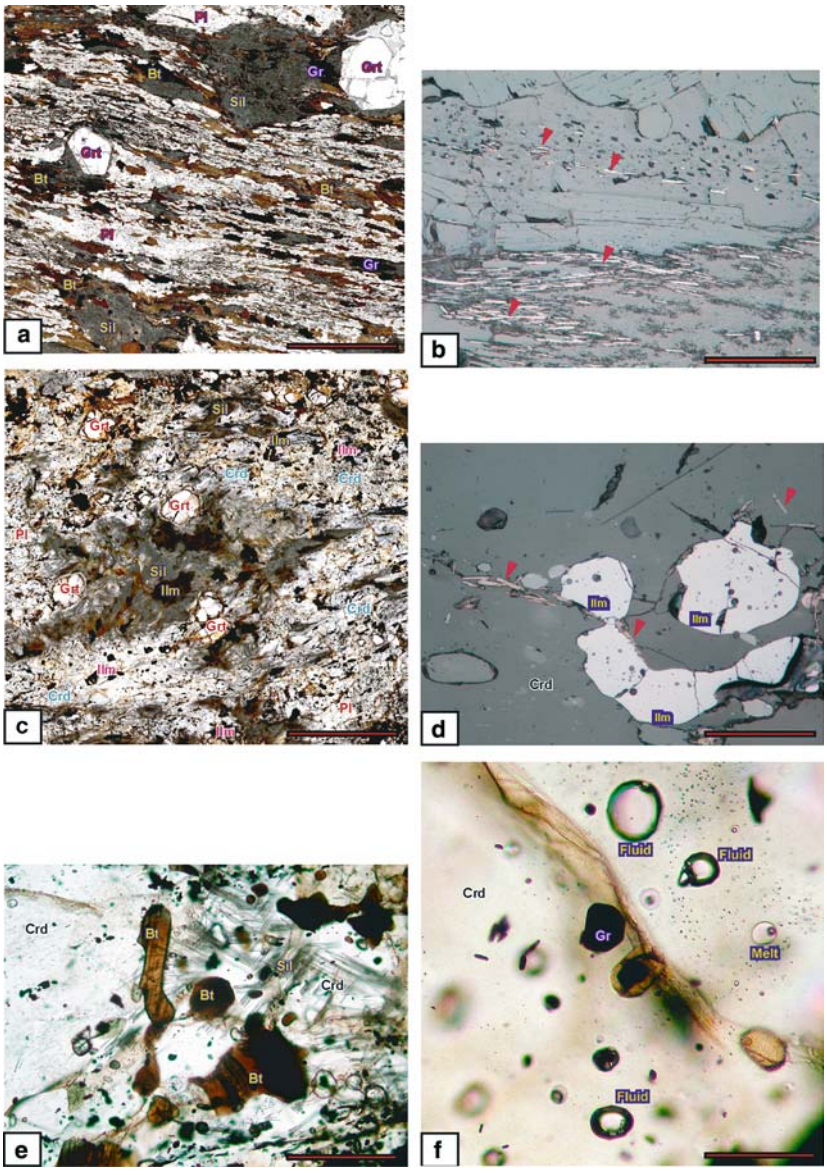

Fig. 1 Petrographic features of the studied samples. (**a**) Thin-section scale photomicrograph of biotite-rich sample HO20. The sample is composed of biotite (Bt), plagioclase (Pl), fibrolitic sillimanite (Sil), graphite (Gr) and melt. Plane-polarised light, scale bar = 0.8 cm; (**b**) reflected-light close-up photomicrograph of (a). The sample contains abundant graphite (*red arrows*). Scale bar = 0.8 mm; (**c**) Thin-section scale photomicrograph of sample AV-HZ8. This rock is almost free of biotite, is made of garnet, cordierite (Crd), plagioclase, sillimanite, ilmenite (Ilm) and graphite, and probably derives from HO20 through biotite melting. Plane-polarised light, scale bar = 0.8 cm; (**d**) Reflected-light close-up photomicrograph of (c). This sample contains both graphite and ilmenite. The small round dark spots within ilmenite are silicate melt inclusions. Scale bar = 0.8 mm; (**e**) Resorbed crystals of biotite included in a single cordierite porphyroblast. Plane-polarised light, scale bar = 0.2 mm; (**f**) Photomicrograph showing immiscible trapping of coexisting fluid (Fluid) and melt inclusions (Melt) in a cordierite crystal (Crd) from sample AV-HZ8. Fluid inclusions contain a CO_2-rich mixture as verified by laser Raman spectroscopy (see text for details). Black platelets of graphite also occur within cordierite. Plane-polarised light, scale bar = 60 μm

Table 1 Full mineral assemblage of the studied samples and summary of microchemical parameters

Sample	Mineral assemblage	Chemical parameters			
		Bt (X_{Fe})	**Grt (X_{Fe})**	**Crd (X_{Fe})**	**Pl (Ab %)**
HO20	Bt-Grt-Sil-Pl-Gr-melt	0.67	0.85		65
HO30	Bt-Grt-Sil-Pl-Gr-melt	0.67	0.85		65
HO50	Bt-Grt-Sil-Pl-Kfs-Crd-Ilm-Gr-melt	0.68	0.87	0.50	61–68
AV-HZ8	Bt† -Grt-Sil-Pl-Kfs-Crd-Ilm-Gr-melt	0.61–0.74	0.85–0.88	0.43–0.61	35–51
HO03	Grt-Sil-Qtz-Crd-Ilm-Gr-melt		0.87	0.50	

†) Rare relicts

extensive phenomena of post-entrapment fluid inclusion modification, the immiscible fluid and melt inclusions indicate that during plagioclase and cordierite growth at high-temperature, a CO_2-rich fluid phase was present and was stable together with granitic melt.

Only the phases listed in Table 1 have been observed in the xenoliths: other Fe-bearing minerals (e.g., magnetite, hercynite, etc.), potentially relevant for the purpose of this paper, have not been detected by any of the adopted analytical techniques.

Analytical techniques

Mineral concentrates were obtained by initial crushing of the rocks followed by short milling in an agate mortar to reach a final grain-size of 125–180 μm. The grinding and milling time did not exceed 5 minutes, and the rock fragments were immersed in ethanol during milling, to reduce oxidation during sample preparation (Dyar and Burns 1986). High purity concentrates (>99%) were obtained by magnetic separation followed by hand picking. The uncertainty about the purity of ilmenite concentrates is slightly higher, due to their opaqueness; zero-background X-ray diffractometry performed after the acquisition of Mössbauer spectra revealed the presence of trace amounts of garnet, cordierite and biotite which are negligible as for the measurement of the Fe^{3+}/Fe_{tot} of ilmenite. Owing to the small size of the melt inclusions (Fig. 1), we were not able to separate and analyse them *ex situ*.

Biotite, garnet, ilmenite and cordierite concentrates were analysed for Fe^{3+}/Fe_{tot} by Mössbauer spectroscopy. We acquired Mössbauer spectra at room temperature using a constant acceleration spectrometer with symmetrical waveform and a ^{57}Co source (nominal strength 1.4 MBq) in a Rh matrix. The finely ground powder was suspended in vaseline, wrapped in a thin plastic foil and inserted in the γ-ray beam. In order to improve the absorption line resolution, the thickness of the Mössbauer absorbers was optimised at about 2.5 mg/cm^2 Fe, so that thickness corrections were not necessary. Biotite spectra displayed asymmetrical doublets, as expected for sheet silicates: this asymmetry is due to preferred orientations of the silicate crystals and reflects the platy morphology of some of them. After data recollection at the so-called ''magic angle'' (the normal to the sample forms an angle of 54.7° with the γ-ray direction), the asymmetry decreased approaching the value of 1. In addition, the spectrum of the ilmenite sample HO50 was collected in the same way because this sample contains also crystals with a platy morphology. Datasets displaying marked asymmetry have been discarded, and only the results of the ''magic angle'' spectra are reported and discussed. Pure Lorentzian line-shapes were employed to fit the spectra, using the ''Recoil'' program (Rancourt and Ping 1991). The hyperfine parameters (isomer shift, IS; quadrupole splitting, QS, and full linewidth at half maximum, W) are expressed in mm/s.

Major element composition of all phases from the five rock samples were obtained on polished thin sections, with a CAMECA Camebax electron microprobe (EMP) of C.N.R., Istituto di Geoscienze e Georisorse, Sezione di Padova. Analytical conditions were 15 kV accelerating voltage and 15 nA beam current, with 10 s peak counting; natural and synthetic silicates and oxides were used as standards, and matrix effects were corrected by the ZAF method. The recalculation of Fe^{3+} from EMP data was done following Droop (1987).

Results

Mössbauer data

The Mössbauer parameters and Fe^{3+}/Fe_{tot} ratios of analysed samples are reported in Table 2. All the samples are characterised by a large amount of Fe^{2+}, recognizable by strong doublets with isomer shifts slightly larger than 1.00 mm/s (Fig. 2). When present, Fe^{3+} species are characterised by weak signals, partially hidden inside the low velocity component of the Fe^{2+} absorption.

The garnet presents a typical absorption, characterised by a wide quadrupole splitting, about 3.50 mm/s, due to octa-coordinated Fe^{2+} (Stevens et al. 1998). The garnet samples are devoid of impurities or oxidation products, with the exception of HO30 and HO50, which show a weak signal related to a Fe^{3+} component. As the Fe^{3+} lines are very weak and partially hidden, the corresponding parameters are affected by large errors; therefore, these lines are not reported in Table 2, even if a $Fe^{3+}/Fe_{tot}=0.01$ is assumed for caution. Traces of Fe^{3+} were also recognised in cordierite from HO50a, whereas the other cordierite specimens present only signals related to Fe^{2+} in octahedral geometry, in agreement with literature data (Khomenko et al. 2001).

Mössbauer spectra of ilmenite from Bt-rich and Bt-free samples are different: HO50 contains an appreciable amount of Fe^{3+}, whereas AV-HZ8 is devoid of ferric iron. In the ilmenite of HO50, zero-background X-ray diffractometry revealed the presence of trace amounts of biotite, cordierite and garnet, which however cannot account for the 6% Fe^{3+}/Fe_{tot} measured by Mössbauer. In addition, EMP analyses do not confirm the presence of significant amounts of Fe^{3+} homogeneously distributed in the crystals (see below), and both optical and scanning electron microscopy did not reveal exsolution textures in ilmenite. Therefore, we infer that the ferric iron detected by Mössbauer spectroscopy, hosted in a highly symmetric octahedral site, is related to the oxidation of some small parts of the ilmenite grains as reported from weathered rocks (Virgo et al. 1988; Waerenborgh et al. 2002). The ilmenite spectrum of sample AV-HZ8 points out the presence of three Fe^{2+} lines; the first line shows parameters close to those of ilmenite in HO50, whereas the second one can be related to a similar site in ilmenite, but more distorted. The third line is given by Fe^{2+} in octahedral geometry (IS: 1.26 mm/s, QS: 2.55 mm/s), probably due to cordierite impurities.

Biotite samples contain an amount of Fe^{3+} varying from 9% to 16%. In all the samples, the three octahedral ferric sites are characterised by rather different values of QS, as a consequence of different site distortions. In addition, the rather high isomer shifts for the Fe^{3+} component is probably due to short Fe-O bonds that imply a high *d* electron density. The measured Mössbauer parameters are in agreement with literature data

Table 2 Mössbauer effect parameters of the examined sample obtained by Lorentzian line profiles. IS isomer shift; QS: quadrupole splitting; W: fullwidth at halfheight, A: relative area. All the values are related to metallic α-iron

Samples	IS (mm/s)	QS (mm/s)	W (mm/s)	A (%)	Fe^{3+}/Fe_{tot}	Attributions
Garnet						
HO20	1.30	3.53	0.17	100	0	Fe^{2+}
HO30	1.28	3.53	0.16	99	≈ 0.01	Fe^{2+}
HO50	1.28	3.51	0.16	99	≈ 0.01	Fe^{2+}
AV-HZ8	1.28	3.49	0.15	100	0	Fe^{2+}
HO03	1.28	3.51	0.12	100	0	Fe^{2+}
Cordierite						
HO50a	1.21	2.31	0.17	99	≈ 0.01	Fe^{2+}
HO50b	1.21	2.28	0.15	100	0	Fe^{2+}
AV-HZ8	1.22	2.29	0.14	100	0	Fe^{2+}
HO03	1.21	2.29	0.16	100	0	Fe^{2+}
Ilmenite						
HO50	1.07	0.65	0.33	94	0.06	Fe^{2+}
	0.31	0.34	0.29	6		Fe^{3+}
AV-HZ8	1.18	0.74	0.36	76	0	Fe^{2+}
	1.02	1.10	0.51	17		Fe^{2+}
	1.26	2.55	0.48	7		Fe^{2+}
Biotite						
HO20	0.58	0.58	0.28	6	0.13	Fe^{3+}
	0.41	1.36	0.32	7		Fe^{3+}
	1.13	2.59	0.24	22		Fe^{2+}
	1.11	2.29	0.30	36		Fe^{2+}
	1.10	1.93	0.40	29		Fe^{2+}
HO30	0.57	0.62	0.28	10	0.16	Fe^{3+}
	0.41	1.41	0.30	6		Fe^{3+}
	1.12	2.58	0.26	21		Fe^{2+}
	1.02	2.28	0.30	36		Fe^{2+}
	1.08	1.93	0.40	27		Fe^{2+}
HO50	0.55	0.55	0.27	5	0.09	Fe^{3+}
	0.40	1.34	0.24	4		Fe^{3+}
	1.25	2.57	0.31	28		Fe^{2+}
	1.11	2.28	0.30	34		Fe^{2+}
	1.09	1.92	0.40	29		Fe^{2+}
AV-HZ8	0.59	0.64	0.38	10	0.14	Fe^{3+}
	0.41	1.47	0.28	4		Fe^{3+}
	1.12	2.66	0.26	20		Fe^{2+}
	1.10	2.36	0.31	33		Fe^{2+}
	1.08	2.01	0.41	33		Fe^{2+}

(Stevens et al. 1998), and indicate a distorted octahedral geometry.

EMP data

We analysed all the phases which are potential carriers of iron, even in minor amounts: biotite, garnet, cordierite, ilmenite, feldspars, sillimanite and melt inclusions; the representative analyses are reported in Tables 3 and 4. As the three Bt-rich samples show the same mineral chemistry, here we report only the data from HO50, the one which also contains Crd, Ilm Pl and Kfs (Table 1).

Biotite data from Bt-rich samples are detailed in Cesare et al. (2003a). Compositions are homogeneous throughout and within the three samples (Table 3), with $X_{Fe} = 0.67–0.68$ and Ti = 0.26–0.29 apfu (apfu = atoms/11 oxygens). The armoured Bt relics in the Bt-poor sample AV-HZ8 have a wider X_{Fe} range (0.61–0.74) and slightly higher Ti (up to 0.33 apfu).

Garnet from HO50 is homogeneous with composition $Alm_{81}Prp_{13}Sps_{02}Grs_{04}$, and with an X_{Fe} of 0.87. Garnet from HO03 ($Alm_{81}Prp_{13}Sps_{03}Grs_{03}$, $X_{Fe} = 0.86$) is identical to the previous sample. Garnet from AV-HZ8 has a slightly more variable composition: $Alm_{79-84}Prp_{11-14}Sps_{01-06}Grs_{02-04}$, with $X_{Fe} = 0.85–0.88$.

Cordierite has similar composition both in the Bt-rich sample HO50 and in the Bt-free HO03. It is homogeneous with $X_{Fe} = 0.50$, very low Na_2O (0.15 wt%) and EMP totals of 99 to 100 wt%. Cordierite from AV-HZ8 has X_{Fe} in the range 0.43–0.61.

EMP analyses of ilmenite were used to estimate the Fe^{3+} content by charge balance (Table 4). All analyses are similar, giving compositions close to stoichiometric $FeTiO_3$. In fact, the Fe^{3+} recalculated from charge balance is negligible (< 0.6% of Fe_{tot}), even considering the analytical errors of the microprobe at > 95% confidence level. While for sample AV-HZ8 these data are in agreement with the Mössbauer results, there seems to be an inconsistency for sample HO50, where Mössbauer indicates 6% Fe^{3+}/Fe_{tot}. As discussed above, we interpret

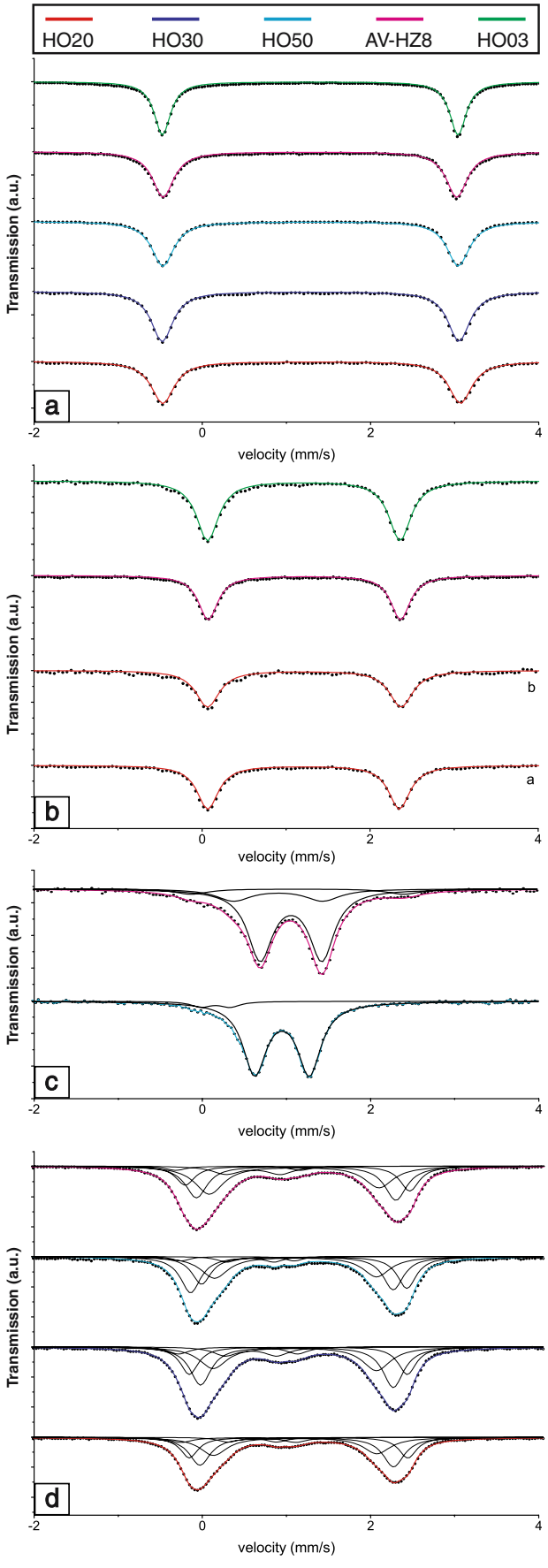

Fig. 2 Room temperature Mössbauer spectra of garnet (**a**), cordierite (**b**), ilmenite (**c**), and biotite (**d**) samples separated from different bulk materials. *Red lines* represent HO20; *blue lines* HO30; *cyan lines* HO50 (a, b sample for cordierite); *magenta lines* AV-HZ8 and *green lines* represent HO03 samples, respectively

such difference between the estimated/measured Fe^{3+} as the result of the different analytical technique employed: the EMP spots were purposely taken away from the rims of the grains, thereby avoiding the parts which are most likely to be affected by oxidation during weathering.

Plagioclase has composition $Ab_{61\text{-}68}An_{26\text{-}38}Or_{03\text{-}06}$ in sample HO50, and is more heterogeneous and calcic ($Ab_{35\text{-}51}An_{42\text{-}63}Or_{02\text{-}05}$) in AV-HZ8. K-feldspar has up to 23 mol% Ab in sample HO50, and up to 18 mol% Ab in AV-HZ8. On average, all feldspars have $<$ 0.1 wt% FeO_{tot}. As feldspars and sillimanite are virtually devoid of iron (FeO_{tot} <0.3 wt%), their contribution to the overall iron content of the xenoliths is negligible.

Melt inclusions have peraluminous (ASI = 1.2), felsic (FeO + MgO $<$ 2 wt%) rhyolitic composition, as generally measured in other melt inclusions from similar xenoliths (Cesare et al. 1997; Cesare et al. 2003b).

Iron reduction during biotite melting

The results of Fe^{3+} measurements indicate two important aspects of the behaviour of ferric iron during high-grade metamorphic processes and partial melting. First, even at reducing conditions defined by the presence of graphite and ilmenite, biotite is a carrier of important amounts of Fe^{3+} in graphitic metapelites. Second, Fe^{3+} displays a systematic partitioning among minerals, so that Fe-bearing phases other than biotite (cordierite, garnet and ilmenite) contain very low amounts of Fe^{3+}. These data fit earlier, though scattered, reports on the Fe^{3+} contents of garnet (e.g., Dyar et al. 2002), cordierite (e.g., Geiger et al. 2000) and ilmenite (e.g., Hand et al. 1994).

One major implication of this study is that the consumption of biotite may represent an important event of iron reduction during crustal melting. Therefore, the results can be employed to evaluate the balance of Fe^{3+} during granulite formation from metapelitic sources. Instead of using the natural reaction (1) we consider a balanced version of the more familiar model biotite melting reaction (e.g., Clemens 1990):

$$Bt + Pl + Qtz + Sil = Grt + Kfs + melt \quad (3)$$

which produces a granulitic restite and a felsic (<1.5 wt% FeO_{tot}) granitic melt. Note that the overall conclusions of this balance are valid regardless of the model reaction considered and of its variance, as long as hematite or magnetite, or other phases not considered in this paper, do not occur in the assemblage.

Table 3 Representative electron microprobe analyses of minerals and glass in the studied samples

Sample	HO50	AV-HZ8	HO50	AV-HZ8	HO03	HO50	AV-HZ8	HO03	HO50	AV-HZ8	HO50	AV-HZ8	HO50	HO50
Phase	Bt	Bt	Grt	Grt	Grt	Crd	Crd	Crd	Pl	Pl	Kfs	Kfs	Sil	melt
FeO	23.44	25.04	37.00	37.59	36.49	11.74	10.05	11.67	0.01	0.13	0.06	0.00	0.20	0.74
Na_2O	0.41	0.32	0.00	0.00	0.00	0.11	0.05	0.16	7.35	5.65	2.32	1.81	0.01	1.72
MgO	6.35	6.03	3.46	3.15	3.41	6.64	7.51	6.55	0.00	0.01	0.00	0.00	0.05	0.11
Al_2O_3	18.84	17.10	20.55	20.47	20.97	32.29	32.61	32.81	24.38	27.11	18.79	18.80	61.83	13.16
SiO_2	34.43	33.70	36.97	37.12	37.25	48.19	48.68	48.29	61.19	56.73	64.93	65.11	36.52	72.68
K2O	8.55	8.79	0.01	0.00	0.00	0.10	0.10	0.07	0.82	0.61	12.03	13.17	0.04	5.58
CaO	0.01	0.00	1.03	1.22	1.07	0.01	0.00	0.05	6.01	9.53	0.17	0.13	0.06	0.30
TiO_2	4.86	5.17	0.01	0.02	0.03	0.00	0.04	0.00	0.02	0.00	0.01	0.00	0.00	0.09
Cr_2O_3	0.06	0.07	0.02	0.04	0.00	0.02	0.02	0.00	0.01	0.05	0.00	0.05	0.01	0.02
MnO	0.04	0.03	1.28	0.63	1.53	0.10	0.31	0.09	0.00	0.00	0.02	0.02	0.00	0.01
Total	**97.04**	**96.26**	**100.34**	**100.24**	**100.74**	**99.20**	**99.36**	**99.69**	**99.80**	**99.83**	**98.32**	**99.10**	**98.72**	**94.40**
#Fe^{+2}	1.53	1.63	5.00	5.08	4.89	1.02	0.86	1.01	0.00	0.01	0.00	-	0.00	
# Na^{+1}	0.06	0.05	–	–	–	0.02	0.01	0.03	0.64	0.49	0.21	0.16	0.00	
# Mg^{+2}	0.74	0.70	0.83	0.76	0.82	1.03	1.15	1.01	–	–	–	–	0.00	
# Al^{+3}	1.73	1.57	3.91	3.90	3.96	3.95	3.95	3.99	1.28	1.44	1.02	1.02	1.99	
# Si^{+4}	2.68	2.62	5.97	6.00	5.97	5.00	5.01	4.98	2.73	2.56	3.00	3.00	1.00	
# K^{+1}	0.85	0.87	0.00	0.00	0.00	0.01	0.01	0.01	0.05	0.04	0.71	0.77	0.00	
# Ca^{+2}	0.00	0.00	0.18	0.21	0.18	0.00	0.00	0.01	0.29	0.46	0.01	0.01	0.00	
# Ti^{+4}	0.29	0.30	0.00	0.00	0.00	0.00	0.00	0.00	0.00	0.00	0.00	0.00	0.00	
# Cr^{+3}	0.00	0.00	0.00	0.01	0.00	0.00	0.00	0.00	0.00	0.00	0.00	0.00	0.00	
# Mn^{+2}	0.00	0.00	0.18	0.09	0.21	0.01	0.03	0.01	0.00	0.00	0.00	0.00	0.00	
X_{Fe}	0.67	0.70	0.86	0.87	0.86	0.50	0.43	0.50						
Alm			0.81	0.83	0.80									
Sps			0.03	0.01	0.03									
Grs			0.03	0.03	0.03									
Pyp			0.13	0.12	0.13									
Ab									0.66	0.50	0.22	0.17		
An									0.30	0.47	0.01	0.01		
Or									0.05	0.04	0.77	0.82		

Cesare et al. "Fe3+ reduction...." Table 3

Table 4 Electron Microprobe Analyses of Ilmenite

Sample	HO 50 (n = 23)*		HO 03 (n = 24)		AV-HZ8 (n = 23)	
	avg.	st.dev.	avg.	st.dev.	avg.	st.dev.
Oxide	(wt%)	(wt%)	(wt%)	(wt%)	(wt%)	(wt%)
SiO_2	0.04	0.02	0.02	0.02	0.02	0.02
TiO_2	53.34	0.46	53.09	0.41	52.84	0.32
Al_2O_3	0.18	0.03	0.15	0.03	0.10	0.04
Cr_2O_3	0.03	0.03	0.03	0.04	0.13	0.06
FeO_t	45.56	0.47	46.28	0.40	45.19	0.37
MnO	0.29	0.07	0.16	0.10	0.79	0.07
MgO	0.89	0.08	0.86	0.12	0.65	0.08
CaO	0.02	0.03	0.01	0.01	0.02	0.01
Total	100.34	0.55	100.60	0.55	99.73	0.41
Atoms (based on 2 cations, 3 oxygens)						
Si	0.001		0.000		0.001	
Ti	1.002		0.995		1.001	
Al	0.005		0.004		0.003	
Cr	0.001		0.001		0.002	
Fe^{3+}	0.000		0.005		0.000	
Fe^{2+}	0.950		0.959		0.951	
Mn	0.006		0.003		0.017	
Mg	0.033		0.032		0.025	
Ca	0.001		0.000		0.000	

* Analyses are reported as average (avg.) and standard deviation (st.dev.) of n. datapoints

The solubility of Fe^{3+} in silicate melts is highly variable (Ottonello et al. 2001) and there are no experimental data directly applicable to the present study. We assume that the Fe^{3+}/Fe_{tot} of our model melt is c. 10%, as measured in rhyolitic glass at 800°C, 2 kbar and f_{O_2} = NNO (Baker and Rutherford 1996). Consider the

partial melting of a rock containing 20 wt% biotite with a composition similar to that of the Bt-rich xenoliths (23 wt% FeO_{tot}, 15% Fe^{3+}/Fe_{tot}, 2.5 wt% H_2O; Cesare et al. 2003a): according to the mass balance proposed by Kriegsman (2001) and modified by Cesare et al. (2003a) to account for dehydrogenation of natural Ti-rich biotite, this rock produces 17 wt% melt (1.5 wt% FeO_{tot}, 10% Fe^{3+}/Fe_{tot}, 3 wt% H_2O at 7 kb, 900°C according to Holtz et al. 2001) and 12 wt% garnet (35 wt% FeO_{tot}, 1% Fe^{3+}/Fe_{tot}). It follows that the Fe_2O_3 in the bulk rock decreases from 0.69 wt% to 0.068 wt%, implying that during granulite formation by biotite melting, 90% of Fe^{3+} in the rock (all in biotite) is reduced to Fe^{2+}.

Owing to the small amounts of Fe in natural anatectic granites, the model is tenable even if the melt had higher Fe^{3+}/Fe_{tot}: in the extreme case that all the Fe of melt was Fe^{3+}, there would be nonetheless an overall reduction of 63% of Fe^{3+} to Fe^{2+}.

Given the low Fe^{3+}/Fe_{tot} ratios of all minerals other than biotite (Table 4) the proposed mechanism of Fe^{3+} reduction during partial melting in the granulite facies is equally valid:

- if cordierite is produced along with garnet, or in place of it, such as in low-pressure, upper crustal granulites (e.g., Vielzeuf and Holloway 1988);
- if ilmenite is taken into consideration as a product of the melting of natural, Ti-rich biotite [e.g., as in reaction (1)].

In addition, because orthopyroxene contains very low amounts of Fe^{3+} (< 1% of Fe_{tot}) in some granulites (Skogby et al. 1992), we propose that Fe^{3+} reduction is likely to occur also in the granulitization of Al_2SiO_5-free graphitic metagreywackes, important constituents of many granulitic terranes (e.g., the Kerala Khondalite Belt, Chacko et al. 1987) by the reaction:

$$Bt + Pl + Qtz = Opx + Kfs + melt \quad (4)$$

CO_2 as the consequence of granulite formation

As free oxygen has extremely low concentrations as a fluid species in natural petrologic systems, the reduction of Fe^{3+} must be accompanied by the concomitant oxidation of another element. In graphitic rocks, the most suitable element for oxidation is carbon, which converts to CO_2. Thus, we can envisage the process of granulitization via biotite melting as accompanied by the model redox reaction:

$$2Fe_2O_3^{(Bt)} + C^{(Gr)} \Rightarrow 4FeO^{(Crd,Grt,Ilm,Opx)} + CO_2^{(fluid,melt,Crd)} \quad (5)$$

Under the model conditions proposed above, this process could oxidise 230 ppm graphite, producing 860 ppm CO_2 in the rock. Therefore the melting of biotite is able to produce a significant amount of CO_2.

The CO_2 can be present as a free fluid only if all the coexisting phases are CO_2-saturated. In partially melted metapelites and metagreywackes, the CO_2-bearing phases are cordierite and the granitic melt, which, at 5 kbar and 900°C, can incorporate up to 0.9 wt% (Harley et al. 2002) and up to 2,500 ppm (Tamic et al. 2001) CO_2, respectively. It follows that in order to model the CO_2 distribution between phases and fluids, i.e., to verify whether the rock becomes CO_2-saturated, one needs to calculate a proper mass balance of the biotite melting reactions. As biotite dehydration melting can produce variable amounts of melt and peritectic phases (cordierite, garnet, orthopyroxene, K-feldspar and ilmenite) depending on P, T and on the composition of the system (particularly X_{Mg}, a_{H_2O}, Al_2O_3), we consider here three scenarios (Fig. 3) which can be envisaged as end-members for the prediction of CO_2 behaviour. The scenarios, which differ essentially for the Fe-Mg peritectic phase produced, are: (a) middle-P (7 kbar) melting of metapelites (Grt production); (b) low-P (5 kbar) melting of metapelites (Crd production); (c) low-P (5 kbar) melting of metagreywackes (Opx production). In all cases the starting material contains 20 wt% Bt, and fluid-absent reaction leads to total biotite melting.

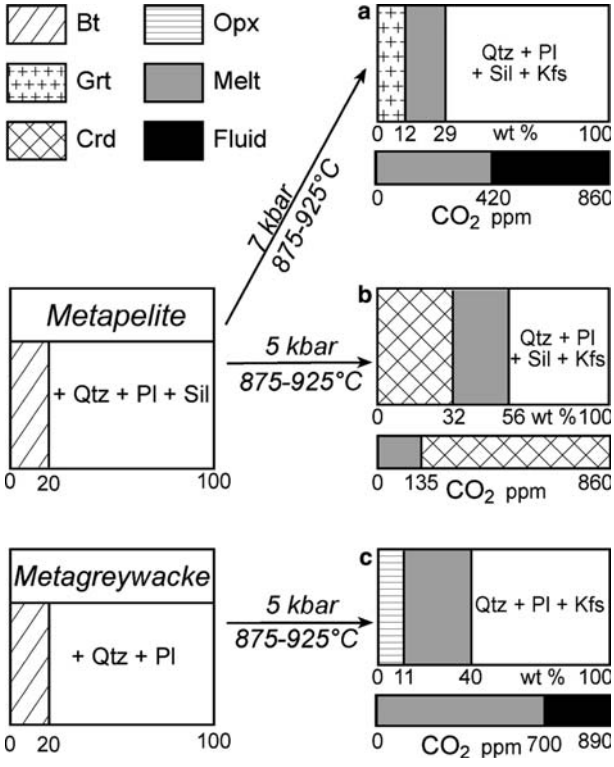

Fig. 3 Schematic illustration of the three biotite dehydration melting scenarios discussed in the text. Boxes on the *left side* represent the two model metapelite and metagreywacke starting materials, both containing 20 wt% biotite and > 250 ppm graphite. On the *right side*, boxes give the proportions of the melting products according to the different cases (a to c), and underlying bars show the partitioning of CO_2 among fluid, melt and cordierite

Case (a) has been introduced above: 20 wt% Bt produces 17 wt% melt, which can incorporate 420 ppm of the total CO_2 (860 ppm). Therefore, in this case 440 ppm CO_2 remain as a free fluid component, and the system is CO_2-saturated. Such an amount of CO_2 would occupy c. 0.13% volume at a density of 1 g cm^{-3}, a volume of the same order of magnitude as porosity, as commonly assumed for high-grade metapelites (e.g., Clemens and Vielzeuf 1987).

Case (b) is modelled using the experimental results of Stevens et al. (1997, composition NBS at 5 kbar), where the melting of c. 20% Bt produces c. 32% Crd and c. 24% melt. As these products can accommodate 3,500 ppm CO_2, no free fluid can be present and the system will be undersaturated. More generally, as 10 wt% Crd is enough to take up all the CO_2 produced by the melting of 20 wt% Bt, it is very likely that most Crd-producing melting reactions will lead to CO_2-undersaturation.

Case (c) is modelled using the experimental results of Patiño Douce and Beard (1995, composition SBG at 5 kbar): the melting of 20 wt% Bt produces 11 wt% Opx and 28 wt% melt. The 890 ppm CO_2 produced are mostly taken up by the melt (700 ppm), but the system remains CO_2-saturated. With increasing pressure, the stoichiometry of melting reactions changes in a way that the process trends towards CO_2-undersaturation. As the Bt/melt proportions may significantly differ among the various melting reactions, in some cases the amount of CO_2 produced by Fe^{3+} reduction may be highly sensitive to the Fe^{3+}/Fe_{tot} ratios in the melt. This is particularly evident in the metagreywacke of case (c), where in the unrealistic case that the melt had $Fe^{3+}/Fe_{tot} = 0.43$, only 690 ppm CO_2 would be produced, leaving the system CO_2–undersaturated.

An interesting aspect of the redox process envisaged here is that in models (a) and (c) the system changes from a fluid-absent to a fluid-present scenario. This might seem counterintuitive, but in the former situation "fluid" denotes the H_2O component (e.g., Thompson 1982), whereas in the latter it refers to CO_2.

Figure 3, schematically representing the three scenarios above, shows the very different ways in which CO_2 can be stored in partially melted metasedimentary granulites and migmatites, and how these rocks can achieve very different degrees of CO_2 saturation. It should be considered that these situations are likely to provide the two extremes (maximum saturation and undersaturation) for the system, and that the behaviour of any other rock undergoing partial melting needs a proper mass balance based on precise reaction stoichiometries and Fe^{3+}/Fe_{tot} measurements.

It is important to remark that regardless of the phases in which CO_2 is stored, and of the actual presence of a free CO_2-rich fluid phase, CO_2 is produced in all of the three melting scenarios discussed above, thereby maintaining the effectiveness of the CO_2 production model proposed here. In low pressure melting of metapelites (case b) most of the CO_2 is stored in cordierite, which will then act as the main CO_2 carrier in the upper crust. Depending on the P-T path and reaction history followed by the Crd-bearing rocks, events of CO_2 release and/or redox reactions involving graphite should be expected in relation to Crd-consuming reactions. Whenever biotite melting and oxidation of graphite result in CO_2-saturation (i.e., in most medium-P metapelites and medium- to low-P metagreywackes), the CO_2 produced and filling the pore spaces may be trapped as fluid inclusions within newly forming peritectic minerals (cordierite, garnet, orthopyroxene, K-feldspar), and as channel volatiles in cordierite. This explains the presence of CO_2-dominated inclusions in calcic plagioclase and cordierite from the Bt-free samples of this study, and is in agreement with the ubiquitous occurrence of primary-trapped CO_2-rich fluid inclusions in granulites (Touret and Hartel 1990; Sarkar et al. 2003). In addition, in the case of CO_2-saturation, phenomena of immiscible trapping as observed in Fig. 1f can also occur.

Because this redox process involving Fe^{3+} and graphite is able to produce a free CO_2-rich fluid, part of such fluid could escape from the granulite, and infiltrate adjacent rocks favouring dehydration and subsolidus charnockitization. It should be recalled, however, that CO_2-rich intergranular fluids have a very low mobility (Watson and Brenan 1987), which makes pervasive infiltration difficult.

Discussion

The genesis of CO_2 by biotite melting in graphitic rocks, preliminarily suggested by Hansen et al. (1987) and qualitatively discussed by Hollister (1988) for the formation of CO_2-rich fluid inclusions in orthopyroxene-bearing migmatites, is here demonstrated on the basis of a sound analytical database.

This process is only one of the several explanations offered for the origin of CO_2 in migmatites and granulites, and is not proposed as applicable to all granulite terranes. In fact, it is well known that: (a) many granulites derive from metaigneous, graphite-free protoliths (compilation in Harley 1989); (b) in many granulites graphite is deposited by fluids after the peak of metamorphism (e.g., Stevens 1997); (c) CO_2 is not the only fluid found in granulites, and brines can be dominant (e.g., Touret and Huizenga 1999); (d) some CO_2 is a product of infiltration from external sources (e.g., Farquhar and Chacko 1991); (e) some CO_2 is late in the metamorphic history of the granulites it occurs within (e.g., Lamb et al. 1987). Notwithstanding all these limitations, the internal origin of CO_2 proposed in this paper turns out to have an important role in graphite-bearing metasedimentary granulites, which are very common in the crust throughout the world (compilation in Harley 1989): examples of large-scale occurrences include South India, Madagascar and Sri Lanka, (e.g., Radhika and Santosh 1995), the Eastern

Ghats, India (e.g., Dharma Rao 2000), the Ivrea Zone (e.g., Schmid and Wood 1976), the Lapland granulite belt (e.g., Korja et al. 1996), Southern Norway, (e.g., Touret 1971); Ukraine (e.g., Shchipanski and Bogdanova 1996), the Ryoke Belt, Japan (e.g., Kawakami and Ikeda 2003), the Adirondacks, USA (e.g., Edwards and Essene 1989), New England, USA (e.g., Guidotti 1970), and the Prydz Bay, Antarctica (e.g., Fitzsimons and Harley 1991). Moreover, it is worth noting that graphite presence may be underestimated, as optically graphite-free rocks can indeed contain small amounts of submicroscopic graphite, detectable only by transmission electron microscopy (Ferraris et al. 2004).

The model presented here can be tested in various ways in natural granulite terranes. One method would be the analysis of Fe^{3+} of bulk rocks across an amphibolite-granulite transition, but this kind of research has been rarely performed in the past. Nonetheless, a few old studies on metapelitic granulites in the Ivrea Zone (Sighinolfi 1968) and in the Adirondacks (Engel and Engel 1958) indicate that Fe^{3+} decreases with increasing metamorphic grade, supporting our conclusions. A complementary test can be provided by carbon isotope characterisation of graphite and CO_2. We expect that if CO_2 originated through Fe^{3+} reduction, it should be in isotopic equilibrium with the graphite of the metasediment, as in many case studies (e.g., Pineau et al. 1981; Vry et al. 1988; Fitzsimons and Mattey 1994). An increase in the abundance of CO_2-rich fluid inclusions across the amphibolite-granulite transition (e.g. Touret 1971) would also be consistent with our model.

Complementary to most interpretations on the origin of CO_2 in granulites, which propose either infiltration from external sources, or casual occurrence in the intergranular fluid, the model arising from this study of Fe^{3+} balance during biotite melting predicts that CO_2 is a natural consequence of granulite formation, provided that graphite is present in the pre-granulitic assemblage. One important difference with usual petrogenetic models is that if CO_2 can form in situ by the redox reaction $2Fe_2O_3 + C \rightarrow 4FeO + CO_2$, there is no need for it to be present prior to biotite melting. Therefore, the presence of pure CO_2 or CO_2–rich fluid inclusions in HT or UHT metamorphic rocks (e.g., Tsunogae et al. 2002; Sarkar et al. 2003) does not necessarily imply that the carbonic fluid was in the rock *before* the peak of metamorphism, or that it infiltrated the rock at peak metamorphic conditions: CO_2 may have formed in a fluid-absent, closed system, as soon as biotite started to decompose. Because CO_2 can be produced by oxidation of graphite even in the absence of melt, our model can explain also some occurrences of the CO_2 component of the fluid in granulites formed during subsolidus biotite breakdown.

By proposing an internal origin of CO_2 as a product of granulitization, we help solve a long-standing petrologic paradox, that is the almost ubiquitous presence of CO_2 in granulites despite CO_2 not being required for granulite formation. With a mechanism of local production, we also overcome the additional problem of the low mobility of CO_2, which is hardly compatible with a pervasive occurrence of CO_2 by intergranular flow (Clemens 1990).

The process outlined in this paper should be taken into account in the modelling of carbon degassing from the lithosphere (e.g., Mörner and Etiope 2000; Kerrick 2001), because it suggests that the amounts of CO_2 released from the degassing mantle—believed to be one of the main sources of CO_2 in granulites (e.g., Newton et al. 1980; Frost and Frost 1987; Clemens 1990)—may be overestimated. Conversely, C recycling from the metasedimentary, non carbonatic, upper crust may increase its importance, as part of the CO_2 of granulites could result from oxidation of graphite originally deposited as organic matter in sediments.

Acknowledgements Funding was provided by the University of Padova (Fondi Progetti Ricerca 2002) and Consiglio Nazionale delle Ricerche (Westmed Euromargins European Science Foundation Eurocore). We thank S. Harley and J. Touret for their thoughtful reviews, J. Connolly, E. Essene, L. Hollister, S. Intento, P. Nimis, and M. Satish-Kumar for comments on an earlier version of the manuscript, R. Carampin and F. Zorzi for assistance with microprobe analysis and X-ray diffractometry, respectively.

References

Baker LL, Rutherford MJ (1996) The effect of dissolved water on the oxidation state of silicic melts. Geochim Cosmochim Acta 60:2179–2187

Brown M (2002) Retrograde processes in migmatites and granulites revisited. J Metamorph Geol 20:25–40

Brown M (2003) Metamorphism. Geotimes Highlights: Discoveries in the Earth Sciences. 22:48–7

Cesare B, Maineri C (1999) Fluid-present anatexis of metapelites at El Joyazo (SE Spain): constraints from Raman spectroscopy of graphite. Contrib Mineral Petrol 135:41–52

Cesare B, Salvioli Mariani E, Venturelli G (1997) Crustal anatexis and melt extraction in the restitic xenoliths at El Hoyazo (SE Spain). Mineral Mag 61:15–27

Cesare B, Cruciani G, Russo U (2003a) Hydrogen deficiency in Ti-rich biotite from anatectic metapelites (El Joyazo - SE Spain): crystal-chemical aspects and implications for high-temperature petrogenesis. Am Mineral 88:583–595.

Cesare B, Marchesi C, Hermann J, Gomez-Pugnaire MT (2003b) Primary melt inclusions in andalusite from anatectic graphitic metapelites: Implications for the position of the Al_2SiO_5 triple point. Geology 31:573–576

Cesare B, Maineri C, Baron Toaldo A, Pedron D (2004) Crustal melting, granite formation and immiscibility with carbonic fluids: a fluid inclusion study of the restitic enclaves from the Neogene Volcanic Province of SE Spain. 32nd Int Geol Congr, Abs Vol 1, abs 86–6, 422–423

Chacko T, Ravindra Kumar GR, Newton RC (1987) Metamorphic conditions in the Kerala (South India) Khondalite Belt: a granulite-facies supracrustal terrain. J Geol 96:343–358

Clemens JD (1990) The granulite - granite connexion. In: Vielzeuf D, Vidal P (eds) Granulites and Crustal Differentiation, Kluwer Academic Publishers, Dordrecht, pp 25–36

Clemens JD (1993) Experimental evidence against CO_2-promoted deep crustal melting. Nature 363:336–338

Clemens JD, Vielzeuf D (1987) Constraints on melting and magma production in the crust. Earth Planet Sci Lett 86:287–306

Dharma Rao CV (2000) Metapelitic migmatites from Pangidi, complex, Eastern Ghats Belt, India. Gondw Res 3:105–117

Droop GTR (1987) A general equation for estimating Fe^{3+} concentrations in ferromagnesian silicates and oxides from microprobe analyses, using stoichiometric criteria. Mineral Mag 51:431–435

Dyar MD, Burns RG (1986) Mössbauer spectral study of ferruginous one-layer trioctahedral micas. Am Mineral 71:955–965

Dyar MD, Lowe EW, Guidotti CV, Delaney JS, (2002) Fe^{3+} and Fe^{2+} partitioning among silicates in metapelites: A synchrotron micro-XANES study. Am Mineral 87:514–52

Edwards RL, Essene EJ (1989) Pressure, temperature and C-O-H fluid fugacities across the amphibolite - granulite facies transition, NW Adirondack Mountains, NY. J Petrol 29:39–73

Engel AE, Engel CG (1958) Progressive metamorphism and granitization of the major paragneiss, Northwest Adirondack Mountains, New York. Part I. Total Rock. Bull Geol Soc of Am 69:1369–1414

Farquhar J, Chacko T (1991) Isotopic evidence for involvement of CO_2-bearing magmas in granulite formation. Nature 354:60–63

Ferraris C, Grobety B, Früh-Green GL, Wessicken R (2004) Intergrowth of graphite within phlogopite from Finero ultramafic complex (Italian, Western Alps): implications for mantle crystallization of primary-texture mica. Eur J Mineral 16:899–908

Fitzsimons ICW, Harley SL (1991) Geological relationships in high-grade gneiss of the Brattstrand Bluffs coastline, East Antarctica. Austr J Earth Sci 38:497–519

Fitzsimons ICW, Mattey DP (1994) Carbon isotope constraints on volatile mixing and melt transport in granulite-facies migmatites. Earth Planet Sci Lett 134:319–328

Frost BR, Frost CD (1987) CO_2, melts and granulite metamorphism. Nature 327:503–506

Geiger CA, Rager H, Czank M (2000) Cordierite III: the site occupation and concentration of Fe^{3+}. Contrib Mineral Petrol 140:344–352

Guidotti CV (1970), The mineralogy and petrology of the transition from the lower to upper sillimanite zone in the Oquossoc area, Maine. J Petrol 11:277–336

Hand M, Scrimgeour I, Powell R, Stüwe K, Wilson CJL (1994) Metapelitic granulites from Jetty Peninsula, east Antarctica: Formation during a single event or by polymetamorphism?. J Metamorph Geol 12:557–573

Hansen EC, Janardhan AS, Newton RC, Pram WKBN, Ravindra Kumar GR (1987) Arrested charnockite formation in South India and Sri Lanka. Contrib Mineral Petrol 96:225–244

Harley SL (1989) The origins of granulites: a metamorphic perspective. Geol Mag 126:215–247

Harley SL, Thompson P, Hensen BJ, Buick IS (2002) Cordierite as a sensor of fluid conditions in high-grade metamorphism and crustal anatexis. J Metamorph Geol 20:71–86

Hollister LS (1988) On the origin of CO_2-rich fluid inclusions in migmatites. J Metamorph Geol 6:467–474

Holtz F, Johannes W, Tamic N, Behrens H (2001) Maximum and minimum water contents of granitic melts generated in the crust; a reevaluation and implications. Lithos 56:1–14

Kawakami T, Ikeda T (2003) Depletion of whole-rock boron controlled by the breakdown of tourmaline and retrograde formation of borosilicates in the Yanai area, Ryoke metamorphic belt, SW Japan. Contrib Mineral Petrol 145:131–150

Kerrick DM (2001) Present and past non-anthropogenic CO_2 degassing from the solid Earth. Rev Geophys 39:565–585

Khomenko VM, Langer K, Geiger CM (2001) Structural locations of the iron ions in cordierite: a spectroscopic study. Contrib Mineral Petrol 141:381–396

Korja T, Tuisku P, Pernu T, Karhu J (1996) Field, petrophysical and carbon isotope studies on the Lapland granulite belt: implications for deep continental crust. Terra Nova 8:48–58

Kretz R (1983) Symbols for rock-forming minerals. Am Mineral 68: 277–279

Kriegsman LM (2001) Quantitative field methods for estimating melt production and melt loss. Phys Chem Earth A 26: 247–253

Lamb WM, Valley JW, Brown PE (1987) Post-metamorphic CO_2-rich fluid inclusions in granulites. Contrib Mineral Petrol 96:485–495

Mörner N-A, Etiope G (2002) Carbon degassing from the lithosphere. Global Planet Change 33:185–203

Newton RC, Smith JV, Windley BF (1980) Carbonic metamorphism, granulites and crustal growth. Nature 288:45–50

Ottonello G, Moretti R, Marini L, Vetuschi Zuccolini M (2001) Oxidation state of iron in silicate glasses and melts: a thermochemical model. Chem Geol 174:157–179

Patiño Douce AE, Beard JS (1995) Dehydration melting of biotite gneiss and quartz amphibolite from 3 to 15 kbar. J Petrol 36:707–738

Peterson JW, Newton RC (1989) CO_2-enhanced melting of biotite-bearing rocks at deep-crustal pressure-temperature conditions. Nature 340:378–380

Pineau F, Javoy M, Behar F, Touret J (1981) La geochimie isotopique du facies granulite du Bamble (Norvege) et l'origine des fluides carbones dans la croute profonde. Bull Mineral 104:630–641

Radhika UP, Santosh M (1995) A comparative study of graphite occurrences in South India, Sri Lanka and Madagascar within East Gondwana. Gondwana Res Group Memoir No 2. Field Sci Pub, Osaka, pp 143–158

Rancourt DG, Ping JY (1991) Voigt-based methods for arbitrary-shape static hyperfine parameter distributions in Mössbauer spectroscopy. Nucl Instr Meth B 58:85–97

Roedder E (1984) Fluid inclusions. MSA Rev Min 12:644

Santosh M (1992) Carbonic fluids in granulites: Cause or consequence? J Geol Soc of India 39:375–399

Sarkar S, Santosh M, Dasgupta S, Fukuoka M (2003) Very high density CO_2 associated with ultrahigh-temperature metamorphism in the Eastern Ghats granulite belt, India. Geology 31:51–54

Schmid R, Wood BJ (1976) Phase relationships in granulitic metapelites from the Ivrea-Verbano zone (Northern Italy). Contrib Mineral Petrol 54:255–279

Shchipanski AA, Bogdanova SV (1996) The Sarmatian crustal segment: Precambrian correlation between the Voronezh Massif and the Ukrainian Shield across the Dniepr-Donets Aulacogen. Tectonophysics 268:109–125

Sighinolfi GP (1968) Rapporto di ossidazione del ferro in una serie metamorfica della Valle Strona (Novara). Schweiz Mineral Petrogr Mitt 48:31–39

Skogby H, Annersten H, Domeneghetti M-C, Molin G, Tazzoli V (1992) Iron distribution in orthopyroxene: A comparison of Mössbauer spectroscopy and X-ray refinement results. Eur J Mineral 4:441–452

Stevens G, (1997) Melting, carbonic fluids and water recycling in thee deep crust: An example from the Limpopo belt, South Africa. J Metamorphic Geol 15:141–154

Stevens G, Clemens JD, Droop TR (1997) Melt production during granulite-facies anatexis: experimental data from 'primitive' metasedimentary protoliths. Contrib Mineral Petrol 128:352–370

Stevens JG, Khasanov AM, Miller JW, Pollak H, Li Z (1998) Mössbauer mineral handbook, Mössbauer Effect Data Center

Tamic N, Behrens H, Holtz F (2001) The solubility of H_2O and CO_2 in rhyolitic melts in equilibrium with a mixed CO_2-H_2O fluid phase. Chem Geol 174:333–347

Thompson AB (1982) Dehydration melting of pelitic rocks and the generation of H_2O-undersaturated granitic liquids. Am J Sci 282:1567–1595

Touret JLR (1971) Le faciès granulite en Norvège méridionale. II Les inclusions fluides. Lithos 4:423–436

Touret JLR (1981) Fluid inclusions in high grade metamorphic rocks. In: Short Course in fluid inclusions: applications to petrology, Hollister, LS, Crawford, ML, Min. Assoc. Canada, Calgary, 182–208

Touret JLR, Dietvorst P (1984) Fluid inclusions in high-grade anatectic metamorphites. J Geol Soc London 140:635–649

Touret JLR, Hartel THD (1990) Synmetamorphic fluid inclusions in granulites. In: Vielzeuf D, Vidal P (eds) Granulites and

Crustal Differentiation, Kluwer Academic Publishers, Dordrecht, pp 397–417

Touret JLR, Huizenga JM (1999) Precambrian intraplate magmatism: high temperature, low pressure crustal granulites. J Afr Earth Sci 28:367–382

Tsunogae T, Santosh M, Osanai Y, Owada M, Toyoshima T, Hokada T (2002) Very high-density carbonic fluid inclusions in sapphirine-bearing granulites from Tonagh Island in the Archean Napier Complex, East Antarctica: implications for CO_2 infiltration during ultrahigh-temperature ($T > 1100°C$) metamorphism. Contrib Mineral Petrol 143:279–299

Valley JW, McLelland J, Essene EJ, Lamb WM (1983) Metamorphic fluids in the deep crust: evidence from the Adirondacks. Nature 20:226–228

Vielzeuf D, Holloway JR (1988) Experimental determination of the fluid-absent melting relations in the pelitic system. Consequences for crustal differentiation. Contrib Mineral Petrol 98:257–276

Vielzeuf D, Schmidt MW (2001) – Melting relations in hydrous systems revisited. Applications to metapelites, metagreywackes and metabasalts. Contrib Mineral Petrol 141:251–267

Vielzeuf D, Clemens JC, Pin C, Moinet E (1990) Granites, granulites and crustal differentiation. In: Vielzeuf D, Vidal P (eds) Granulites and Crustal Differentiation. Kluwer Academic Publishers, Dordrecht, pp 59–85

Virgo D, Luth WR, Moats MA, Ulmer GC (1988) Constrains on the oxidation state of the mantle: An electrochemical and ^{57}Fe Mössbauer study of mantle-derived ilmenite. Geochim Cosmochim Acta 52:1781–1794

Vry J, Brown PE, Valley JW, Morrison J (1988) Constraints on granulite genesis from carbon isotope compositions of cordierite and graphite. Nature 332:66–68

Waerenborgh JC, Figueiras J, Mateus A, Gonçalves M (2002) Nature and mechanism of ilmenite alteration: a Mössbauer and X-ray diffraction study of oxidised ilmenite from the Beja-Acebuches Ophiolite Complex (SE Portugal). Mineral Mag 66:421–430

Watson EB, Brenan JM (1987) Fluids in the lithosphere, 1 Experimentally determined wetting characteristics of CO_2-H_2O fluids, their implications for fluid transport, host-rock physical properties, and fluid inclusion formation. Earth Planet Sci Lett 85:497–515